



Modeling of two-step CO oxidation light-off on Pt/γ-Al₂O₃ in the presence of C₃H₆ and NO_x

Adéla Buzková Arvajová, Jan Březina, Rudolf Pečinka, Petr Kočí*

University of Chemistry and Technology, Prague, Department of Chemical Engineering, Technická 5, 166 28 Prague, Czech Republic



ARTICLE INFO

Keywords:

Automotive exhaust gas aftertreatment
Pt/γ-Al₂O₃ catalyst
CO oxidation
Hydrocarbon inhibition
Mathematical modeling

ABSTRACT

Abatement of pollutants in automotive exhaust converters can be negatively affected by interactions of reaction intermediates with the catalyst surface. This paper focuses on a specific inhibition of CO oxidation on Pt/γ-Al₂O₃ catalyst by C₃H₆ oxidation intermediates, leading to a so-called two-step CO light-off behavior. Two reaction pathways contributing to a temporary decrease of CO conversion during a temperature-programmed co-oxidation of CO and C₃H₆ are identified: (i) accumulation of C₃H₆ oxidation intermediates on the catalyst surface that block active sites and progressively inhibit both CO oxidation and total C₃H₆ oxidation, and (ii) CO by-product formation during propylene oxidation. The latter pathway seems to play a minor role while the inhibition effect dominates. The phenomenon is most pronounced at lower (nearly stoichiometric) oxygen concentrations and in the presence of NO. This indicates that the initial formation of C₃H₆ oxidation intermediates is less sensitive to O₂ and NO concentrations, while the total oxidation steps depend more strongly on the actual exhaust gas composition. A novel global reaction kinetic model is proposed that captures all the experimentally observed phenomena including transient accumulation of the reaction intermediates on the catalyst surface and the resulting impact on CO and C₃H₆ conversion. The developed model covers a wide range of operating conditions, from three-way catalyst (stoichiometric mixture) to diesel oxidation catalyst (lean mixture).

1. Introduction

Oxidation of CO and hydrocarbons in catalytic monolith converters has been studied widely over the past decades [1–10]. These reactions together with NO_x reduction and soot filtration represent crucial steps in the automotive exhaust gas aftertreatment technology. In recent years, substantial effort has been devoted to increasing the efficiency of internal combustion engines and minimizing NO_x and soot production. One available way to achieve these objectives is a so-called low-temperature combustion (LTC) as an alternative to conventional modes of internal combustion [11]. The most common forms of LTC are pre-mixed-charge compression-ignition (PCCI) [12], homogeneous-charge compression-ignition (HCCI), reactivity-controlled compression-ignition or low-temperature combustion of diesel-like fuels ensured by an exhaust gas re-circulation system (EGR) [13]. These technologies enable a simultaneous minimization of soot and nitrogen oxides emissions. However, at the same time, CO and hydrocarbon emissions can increase significantly due to relatively lower fuel combustion temperature [13]. The lower temperature of exhaust gas introduces further difficulties to catalytic exhaust gas aftertreatment, as the reaction rates

exponentially decrease with temperature. With regard to this fact, catalytic oxidation of CO and hydrocarbons is nowadays put at the forefront of research again.

The commonly used catalysts for CO and hydrocarbon oxidation are based on Pt and/or Pd supported by γ-Al₂O₃ and/or cerium oxides. Co-oxidation of CO and hydrocarbons exhibits a competitive adsorption of these two species on active surface resulting in a slow-down of the individual reactions in a complete gas mixture [1,4]. Besides this well-known mutual inhibition effect, a non-trivial interactions between CO and C₃H₆ have been reported [6,7]. Hazlett and Epling [6] studied an influence of C₃H₆ on co-current CO and C₃H₆ oxidation over Pt/γ-Al₂O₃ at high concentrations of reactants typical for LTC engines. By the means of diffuse reflectance infra-red Fourier transform spectroscopy (DRIFTS), they revealed surface ethylene and formaldehyde formation in the first step and acetates in the second step of C₃H₆ oxidation. The surface intermediates formation was reflected in both CO and C₃H₆ light-off curve as an inflection, or step, where the reaction rate was slowed down by increasing the surface occupation. A similar effect of partial propylene oxidation was also observed on Pt/γ-Al₂O₃, Pd/γ-Al₂O₃ and bimetallic PtPd/γ-Al₂O₃ catalysts [7]. Traces of

* Corresponding author.

E-mail address: petr.koci@vscht.cz (P. Kočí).

URL: <http://www.vscht.cz/monolith> (P. Kočí).

Table 1
Inlet gas composition used in the experiments and simulations.

Component	Mole fraction y^{in}
CO	0/1660 ppm
C_3H_6	0/860 ppm
NO	0/300/600 ppm
O_2	0.387/0.440/0.823/6.584 %
CO_2	7 %
H_2O	7 %
N_2	Balance

propylene oxidation by-products such as acetone, ethylene, acet-aldehyde, acetic acid, formaldehyde and CO were detected during the light-off. The largest inhibition was observed on Pt catalyst due to a sensitivity of Pt to CO poisoning [7]. Catalyst deactivation effects caused by propylene partial oxidation were recently also described by Herrmann et al. [10].

Mathematical models of catalytic converters for CO and hydrocarbons oxidation developed over the past decades [1–3,5,9,14–19] became standard tools in the design and optimization of automotive exhaust gas aftertreatment systems. Historically, hydrocarbon fragments and intermediates on the catalyst surface have been included in microkinetic models [17,20–24]. The micro-kinetic model [24] considered surface intermediates formation during CO oxidation in the presence of propylene or H_2 , although the particular species reported by Hazlett et al. were not involved [6,7]. However, none of the kinetic models published so far dealt with a strong inhibition effect of C_3H_6 oxidation intermediates on CO oxidation, resulting in a more complex type of CO light-off curve with a plateau or even temporary decrease in CO conversion with increasing temperature as observed in our study. Herein, we present a global kinetic model of an oxidation catalyst extended by the mechanism of surface intermediates formation during C_3H_6 oxidation that is able to describe and predict the experimentally observed phenomena, while keeping a low number of additional reactions and parameters.

2. Experimental set-up

Experiments were performed in a nearly isothermal mini-reactor that contained model Pt/ γ - Al_2O_3 catalyst coated on a 400 cpsi ceramic monolith with platinum loading of 80 g/ ft^3 provided by Johnson Matthey. The tested monolith sample had rectangular shape with dimensions 0.5 cm (height) \times 3 cm (width) \times 3 cm (length). Thermocouples were placed at the inlet and closely to the outlet of the catalyst sample. The inlet mixture was prepared from individual synthetic gases using mass flow controllers (Bronkhorst). The outlet concentrations were measured by FTIR analyzer (MKS 2030HS), mass spectrometer (Hiden QGA) and paramagnetic O_2 analyzer (ABB Optima Magnos 16) with the sampling period 1 s.

The catalyst sample was preconditioned at 550 °C by cycling of 10s-long periods of rich (5 % CO, 1000 ppm C_3H_6) and lean (8 % O_2 , 100 ppm C_3H_6) mixture with constant inlet of 7 % CO_2 , 7 % H_2O and 500 ppm NO for 1 h prior to the experimental part. Before each experiment,

the catalyst was treated for 3 min by switching between oxidizing (5 % O_2) and reducing (2 % H_2) atmosphere at 400 °C in order to clear the surface from all residual hydrocarbon intermediates as well as adsorbed nitrogen oxides. The catalyst was then cooled down in nitrogen to the starting temperature of the experiment. Selected light-off experiments were also repeated with the catalyst cooled down in air to check the possible influence of PtO_x on CO and C_3H_6 oxidation. No noticeable change in the light-off behavior was observed, which is in agreement with the known ability of CO and C_3H_6 to reduce PtO_x [25].

The examined inlet concentrations of individual gas components are listed in Table 1. The oxygen concentration was varied in a wide range in order to cover both Diesel (lean) and gasoline (stoichiometric) engine conditions. The flow rate was 4.23 dm^3/min resulting in the space velocity 50 000 h^{-1} at standard temperature and pressure. Temperature ramps were performed with the rate 5 K/min.

3. Mathematical model

Standard 1D heterogeneous model with plug flow was employed to solve transport and reaction processes in the monolith channel [3]. Mass balances in the flowing gas, mass balances in the pores of catalytic layer, mass balances on the catalyst surface sites, enthalpy balance of the flowing gas, and enthalpy balance of the solid phase are considered in the model [3]. The reaction heat released during the experiments was to a large extent dissipated into steel body of the reactor. Nevertheless, the catalyst was not perfectly isothermal and the maximum measured rise of the outlet temperature after the reaction light-off was approximately 20 K. On account of this fact, standard enthalpy balance of the catalyst solid phase was solved with the heat transfer to the surroundings, using effective heat loss coefficient of 200 W/(m^2K) [3] so that the measured and simulated outlet temperatures matched well.

An extended global reaction kinetic model was developed with the following objectives: (i) to consistently capture the experimentally observed phenomena during co-oxidation of CO and C_3H_6 , particularly the two-step CO light-off behavior, (ii) to keep compatibility with the existing standard global kinetic models, and (iii) to minimize the number of additional reactions and parameters.

Standard reactions and their rate laws in commonly used in global mathematical models of oxidation and three-way catalysts [1,2,5] are listed in Table 2, with the inhibition terms defined in Table 3. Temperature-dependent reaction rate coefficients k_j are calculated using the Arrhenius equation

$$k_j = A_j \exp\left(\frac{-E_{a,j}}{R^g T}\right), \quad 0$$

where j is index of reaction, A pre-exponential factor and E_a activation energy of reaction. The inhibition coefficients $K_{\text{inh},l}$ are calculated as

$$K_{\text{inh},l} = A_{\text{inh},l} \exp\left(\frac{E_{\text{inh},l}}{T}\right), \quad 0$$

where l is index of inhibition coefficient, A_{inh} pre-exponential factor and E_{inh} exponential factor of inhibition. Local component mole fractions y and surface coverages ψ in the catalytic layer are used for the

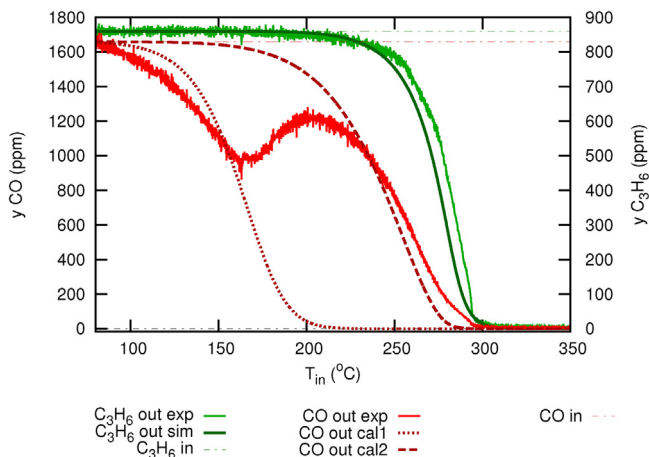
Table 2
Standard reactions and rate laws commonly used in global models of oxidation and three-way catalysts.

No.	Reaction	Rate law
1	$\text{CO} + \frac{1}{2}\text{O}_2 \rightarrow \text{CO}_2$	$R_1 = k_1 \Psi_{\text{Pt}}^{\text{cap}} y_{\text{CO}} y_{\text{O}_2}^{\beta_1} / G_1$
2	$\text{C}_3\text{H}_6 + \frac{9}{2}\text{O}_2 \rightarrow 3\text{CO}_2 + 3\text{H}_2\text{O}$	$R_2 = k_2 \Psi_{\text{Pt}}^{\text{cap}} y_{\text{C}_3\text{H}_6} y_{\text{O}_2}^{\beta_1} / G_1$
3	$\text{NO} + \frac{1}{2}\text{O}_2 \rightleftharpoons \text{NO}_2$	$R_3 = k_3 \Psi_{\text{Pt}}^{\text{cap}} [y_{\text{NO}} y_{\text{O}_2}^{0.5} - y_{\text{NO}_2} / K_{\text{y},2}^{\text{eq}}] / G_2$
4	$\text{NO} + \text{CO} \rightarrow \text{CO}_2 + \frac{1}{2}\text{N}_2$	$R_4 = k_4 \Psi_{\text{Pt}}^{\text{cap}} y_{\text{NO}}^{0.5} y_{\text{CO}} / G_3$
5	$\text{NO} + \frac{1}{9}\text{C}_3\text{H}_6 \rightarrow \frac{1}{3}\text{CO}_2 + \frac{1}{2}\text{N}_2 + \frac{1}{3}\text{H}_2\text{O}$	$R_5 = k_5 \Psi_{\text{Pt}}^{\text{cap}} y_{\text{NO}}^{0.5} y_{\text{C}_3\text{H}_6} / G_3$

Table 3

Inhibition terms employed in the rate laws.

No.	Inhibition term
1	$G_1 = (1 + K_{inh,1}y_{CO} + K_{inh,2}y_{C_3H_6})^2(1 + K_{inh,3}y_{NO_x}^{0.7})T$
2	$G_2 = (1 + K_{inh,4}y_{CO} + K_{inh,5}y_{C_3H_6})^2(1 + K_{inh,6}y_{NO_x}^{0.7})T$
3	$G_3 = (1 + K_{inh,7}y_{O_2})$
4	$G_4 = (1 + K_{inh,8}y_{CO} + K_{inh,9}y_{C_3H_6})^2(1 + K_{inh,10}y_{NO_x}^{0.7})T$
5	$G_5 = (1 + K_{inh,11}y_{CO} + K_{inh,12}y_{C_3H_6})^2(1 + K_{inh,13}y_{NO_x}^{0.7})T$
6	$G_6 = (1 + K_{inh,14}y_{CO} + K_{inh,15}y_{C_3H_6})^2(1 + K_{inh,16}y_{NO_x}^{0.7})T$

**Fig. 1.** Two possible calibrations (cal1 and cal2) of CO oxidation of propylene in a nearly stoichiometric mixture, inlet: 1660 ppm CO, 860 ppm C₃H₆, 0.412 % O₂, 600 ppm NO, 7 % H₂O, 7 % CO₂, balance N₂.

evaluation of reaction rates. Ψ_{Pt}^{cap} denotes the concentration of active Pt sites in the catalytic layer (mol m⁻³). The reaction rates are evaluated in the units of mol m⁻³ s⁻¹, per volume of catalytic coating in monolith.

The terms G defined in **Table 3** represent mutual inhibition effect of CO, C₃H₆ and NO on the reaction rates and their form follows the kinetic model proposed by Voltz et al. [1] and further modified by Oh and Cavendish [2]. In our work, we omitted the term $(1 + K_{inh}y_{CO}y_{C_3H_6})^2$ that was originally included in G_1 by Voltz et al. [1] to embrace the inhibition at extremely high concentrations of CO and C₃H₆. We found this term redundant in the studied range of concentrations relevant for the exhaust gas composition of current engines.

To capture the two-step CO light-off behavior observed on Pt/γ-Al₂O₃ in the complete mixture with C₃H₆, however, this basic set of reactions with standard kinetics is insufficient. It can be seen in **Fig. 1**.

that the outlet CO concentration decreases with temperature up to 160 °C but then it starts to increase, suggesting a negative apparent activation energy and decreasing reaction rate. Only above 200 °C, the outlet CO concentration returns back to the original decreasing trend and approaches eventually zero so that the complete conversion is reached. With the standard model represented by reactions in **Table 2**, it is not possible to capture such a complex behavior and it is necessary to choose between the two limit calibrations describing either the first or the second light-off step (see **Fig. 1**). Note that the difference in the CO light-off temperature for these two cases in **Fig. 1** is more than 80 °C. Therefore, we propose an extension of the standard kinetic model as summarized in **Table 4**.

When comparing the newly proposed kinetics (**Table 4**) with the standard one (**Table 2**), it can be seen that the original rate laws R_1 – R_5 are extended by the term $(1 - \psi_{HCOO}^*)$ that accounts for the decreasing number of available catalytic sites due to the accumulation of hydrocarbon oxidation intermediates on the catalyst surface. Although several different species including ethylene and acetates have been found to form on the catalyst surface during C₃H₆ oxidation [6,7], for the purpose of global kinetics we consider only one model intermediate (HCOO^{*}) that represent their sum. The formation of intermediates during C₃H₆ oxidation is described by the reaction R_6 added in **Table 4**. Total oxidation of the intermediates that can recover the blocked Pt sites is represented by the reaction R_7 . Furthermore, propylene partial oxidation can also lead to CO by-product formation [6,7] which is considered in reaction R_8 . The extended model therefore involves two pathways that both can lead to the increase of the outlet CO concentration: (i) formation of hydrocarbon intermediates (R_6 and R_7) that can block catalytic sites and inhibit the other reactions (R_1 – R_5), and (ii) formation of CO as a by-product of the hydrocarbon oxidation (R_8). The relative importance of the two pathways will be discussed in the following section.

The lab reactor data were utilized to evaluate kinetic parameters of the proposed global kinetic model. The initial estimates were optimized by the simplex minimization method, using weighted least squares of differences between the measured and simulated outlet concentrations as the objective function. The resulting kinetic parameters of the extended model are listed in **Table 5**. The concentration of active Pt sites Ψ_{Pt}^{cap} in Pt/γ-Al₂O₃ coating was calculated from the values determined in [26].

4. Results and discussion

To reveal the importance of CO formation via reaction R_8 in **Table 4**, C₃H₆ oxidation was studied first without co-feeding CO. **Fig. 2a** shows C₃H₆ light-off at nearly stoichiometric oxygen concentration. The C₃H₆ curve is smooth and the outlet concentration decreases gradually with increasing temperature. Only few ppm CO is detected during C₃H₆

Table 4

Extended set of reactions and rate laws including C₃H₆ oxidation intermediates on the catalyst surface (represented in global approximation by HCOO^{*}).

No.	Reaction	Rate law
1	CO + $\frac{1}{2}O_2 \rightarrow CO_2$	$R_1 = k_1 \Psi_{Pt}^{cap} (1 - \psi_{HCOO}^*) y_{CO} y_{O_2}^{\beta_1} / G_1$
2	C ₃ H ₆ + $\frac{9}{2}O_2 \rightarrow 3CO_2 + 3H_2O$	$R_2 = k_2 \Psi_{Pt}^{cap} (1 - \psi_{HCOO}^*) y_{C_3H_6} y_{O_2}^{\beta_1} / G_1$
3	NO + $\frac{1}{2}O_2 \rightleftharpoons NO_2$	$R_3 = k_3 \Psi_{Pt}^{cap} [y_{NO} y_{O_2}^{0.5} - y_{NO_2} / K_{N_2O_2}^{eq}] / G_2$
4	CO + NO → CO ₂ + $\frac{1}{2}N_2$	$R_4 = k_4 \Psi_{Pt}^{cap} (1 - \psi_{HCOO}^*) y_{NO}^{0.5} y_{CO} / G_3$
5	$\frac{1}{9}C_3H_6 + NO \rightarrow \frac{1}{3}CO_2 + \frac{1}{2}N_2 + \frac{1}{3}H_2O$	$R_5 = k_5 \Psi_{Pt}^{cap} (1 - \psi_{HCOO}^*) y_{NO}^{0.5} y_{C_3H_6} / G_3$
6	C ₃ H ₆ + $\frac{15}{4}O_2 + 3Pt \rightarrow 3HCOO^*Pt + \frac{3}{2}H_2O$	$R_6 = k_6 \Psi_{Pt}^{cap} (1 - \psi_{HCOO}^*) y_{C_3H_6} y_{O_2}^{\beta_2} / G_4$
7	$3HCOO^*Pt + \frac{3}{4}O_2 \rightarrow 3CO_2 + \frac{3}{2}H_2O + 3Pt$	$R_7 = k_7 \Psi_{Pt}^{cap} \psi_{HCOO}^* y_{O_2}^{\beta_1} / G_5$
8	C ₃ H ₆ + 3O ₂ → 3CO + 3H ₂ O	$R_8 = k_8 \Psi_{Pt}^{cap} y_{C_3H_6} y_{O_2}^{\beta_2} / G_6$

Table 5
Values of kinetic parameters in the extended kinetic model.

Rate coefficients	A (s ⁻¹)	E_a (kJ mol ⁻¹)
k_1	1.7×10^{17}	70
k_2	1.7×10^{20}	110
k_3	2.0×10^{10}	45
k_4	4.0×10^{14}	70
k_5	1.0×10^{18}	100
k_6	3.5×10^{12}	50
k_7	1.2×10^9	60
k_8	1.7×10^{15}	90
Inhibition coefficients	A_{inh} (1)	E_{inh} (K)
$K_{inh,1}$	6.0×10^1	1000
$K_{inh,2}$	8.0×10^1	1000
$K_{inh,3}$	3.0×10^3	-500
$K_{inh,4}$	1.0×10^2	1100
$K_{inh,5}$	1.0×10^2	2000
$K_{inh,6}$	2.0×10^3	-2000
$K_{inh,7}$	2.5×10^8	-8000
$K_{inh,8}$	3.0×10^1	1000
$K_{inh,9}$	4.0×10^2	1000
$K_{inh,10}$	3.0×10^3	-500
$K_{inh,11}$	2.0×10^1	1000
$K_{inh,12}$	5.0×10^0	1000
$K_{inh,13}$	1.0×10^5	-1500
$K_{inh,14}$	3.0×10^1	1000
$K_{inh,15}$	3.0×10^2	1000
$K_{inh,16}$	1.5×10^3	-500
O ₂ rate orders	Value (1)	
β_1	1.0	
β_2	0.7	
Pt sites concentration	Value (mol m ⁻³)	
Ψ_{Pt}^{cap}	30	

ignition as a consequence of partial oxidation described by the reaction R_8 in Table 4. This is in line with the observations of Hazlett et al. [7] that CO by-product is formed on the Pt/γ-Al₂O₃ catalyst surface due to the lack of adsorbed oxygen. At higher O₂ concentrations tested in this study, this CO formation disappears and only CO₂ is detected as a product of total oxidation.

The inhibiting effect of NO_x on C₃H₆ oxidation can be observed in Fig. 2b. In the presence of NO, the onset of the reaction is moved towards higher temperature by ca 70 °C. Furthermore, the partial C₃H₆ oxidation leading to CO production is more pronounced, which indicates that NO has a stronger inhibition effect on the total propylene oxidation to CO₂ (R_2) than on the partial oxidation leading to CO peak (R_8). This is reflected in the values of inhibition parameters in Table 5. Moreover, the quantity of the formed CO in Fig. 2b is still much lower than it would be necessary to explain the behavior observed in Fig. 1 solely by the reaction R_8 . This suggests that the pathway involving inhibition of CO oxidation by the surface intermediates plays a major role in the two-step CO light-off effect.

To prove this hypothesis, dedicated experiments have been performed for the quantification of CO oxidation inhibition by the intermediates formed during partial oxidation of C₃H₆. Dynamics of the intermediates formation was studied with a full mixture during temperature ramp with inserted isothermal period, Fig. 3. The temperature ramp was stopped for 30 minutes at the point, at which CO oxidation began to slow down. In the first 10 minutes of the isothermal phase, the CO conversion decreased rapidly and only afterwards levelled off. This result demonstrates that at a constant temperature, the catalyst surface becomes progressively occupied by the C₃H₆ oxidation intermediates until steady state is reached. Dynamics and equilibrium of this process

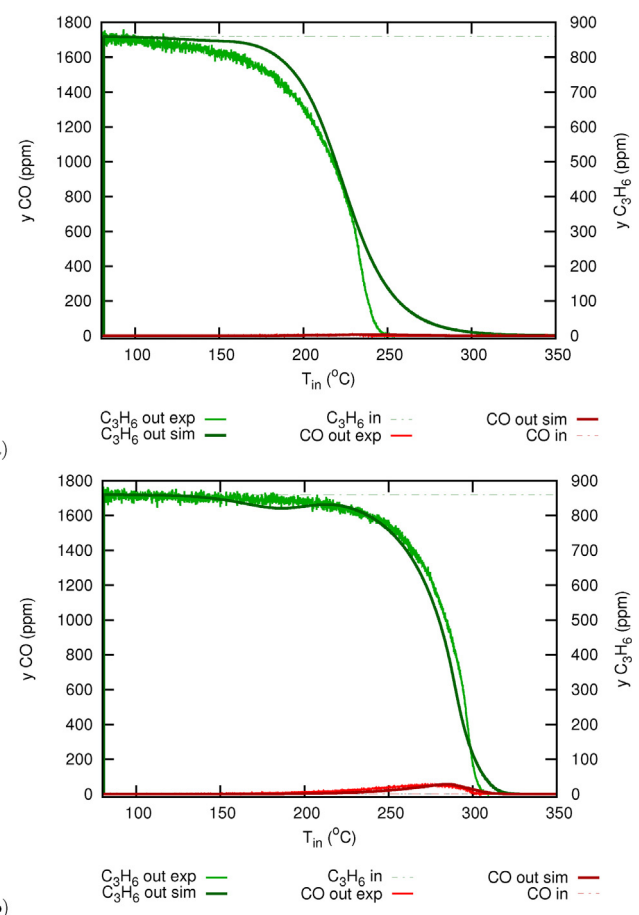


Fig. 2. Propylene oxidation with a nearly stoichiometric amount of O₂ (a) in the absence of NO, (b) in the presence of NO. Feed gas composition: 860 ppm C₃H₆, 0.387 % O₂, 0/600 ppm NO, 7 % H₂O, 7 % CO₂, balance N₂.

is governed by the reactions R_6 and R_7 in Table 5. It can be seen in Fig. 3 that the evolution of the outlet CO concentration during this experiment is described well by the model. The magnitude of this gradual inhibition effect on CO oxidation rate is larger than that of CO by-product formation, as seen from the comparison of Figs. 3 and 2, respectively, which confirms our hypothesis about the relative importance of the two reaction pathways.

Further experiments were arranged to explore the effect of O₂ and NO content in the feed. It was found that magnitude of the two-step CO oxidation light-off phenomenon is largely influenced by both oxygen concentration and the presence of NO. Figs. 4–6 show the results for three different oxygen concentrations, from nearly stoichiometric to a highly lean mixture with large O₂ excess. It can be seen that the magnitude of CO peak on the light-off curve decreases with the increasing oxygen concentration but the residual CO shoulder appears even at the highest oxygen concentration (Fig. 6). For all oxygen concentrations, the phenomenon is exaggerated if NO is present (Figs. 4b–6b). Both experiments and simulations show that the effect is strong both at higher and lower NO concentrations (Fig. 5c). In the absence of NO (Figs. 4a–6a), the effect is considerably smaller but still detectable. The proposed reaction kinetic model captures the observed trends quite well, considering the wide range of examined oxygen concentrations.

NO_x conversions during nearly stoichiometric and lean temperature ramps are shown in Fig. 7a and b, respectively. These results correspond to co-oxidation of CO and propylene reported in Figs. 4b and 5b, respectively. Although the prediction of NO oxidation and NO_x reduction is not a primary goal of our study, the model provides satisfactory results. While full NO_x reduction is achieved in stoichiometric mixture

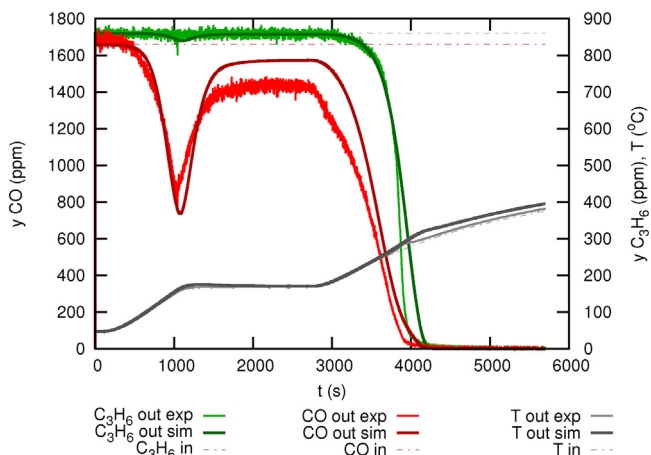


Fig. 3. Temperature-programmed co-oxidation of propylene and CO with inserted isothermal period at 180 °C. Feed gas composition: 1660 ppm CO, 860 ppm C₃H₆, 0.8232 % O₂, 600 ppm NO, 7 % H₂O, 7 % CO₂, balance N₂.

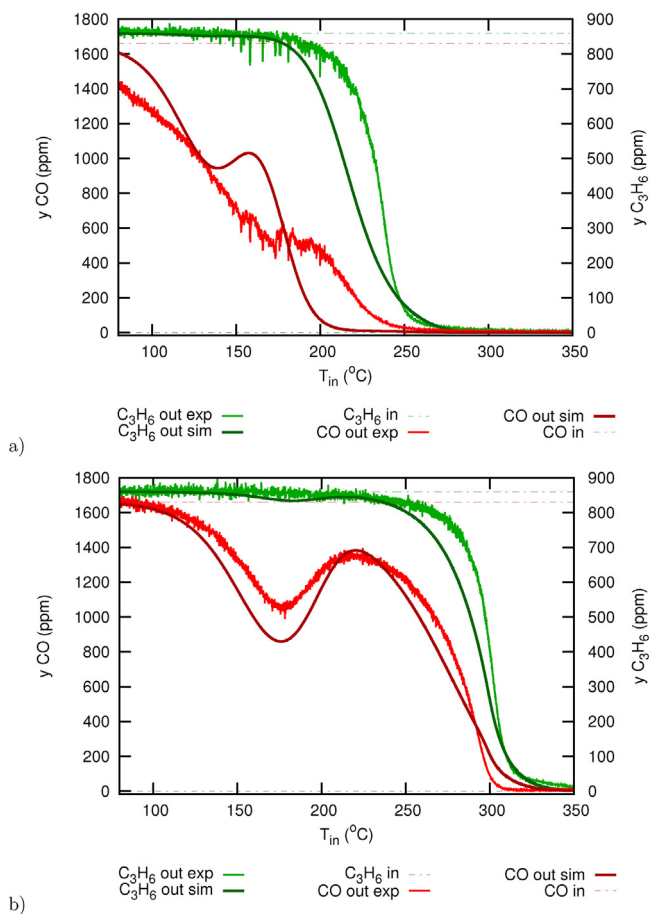


Fig. 4. Co-oxidation of propylene and CO with nearly stoichiometric amount of O₂ (a) in the absence of NO, (b) in the presence of NO. Feed gas composition: 1660 ppm CO, 860 ppm C₃H₆, 0.440 % O₂, 0/600 ppm NO, 7 % H₂O, 7 % CO₂, balance N₂.

above the light-off (Fig. 7a), only partial reduction is observed in the lean mixture, showing also NO oxidation to NO₂ (Fig. 7b).

The measured irregular oscillations in Figs. 5 and 6 were observed repeatedly in experiments under these operating conditions and can be attributed to the transient nature of CO and C₃H₆ oxidation on Pt sites. The oscillatory behavior of these reactions in a certain range of concentrations has been confirmed both by experiments and microkinetic

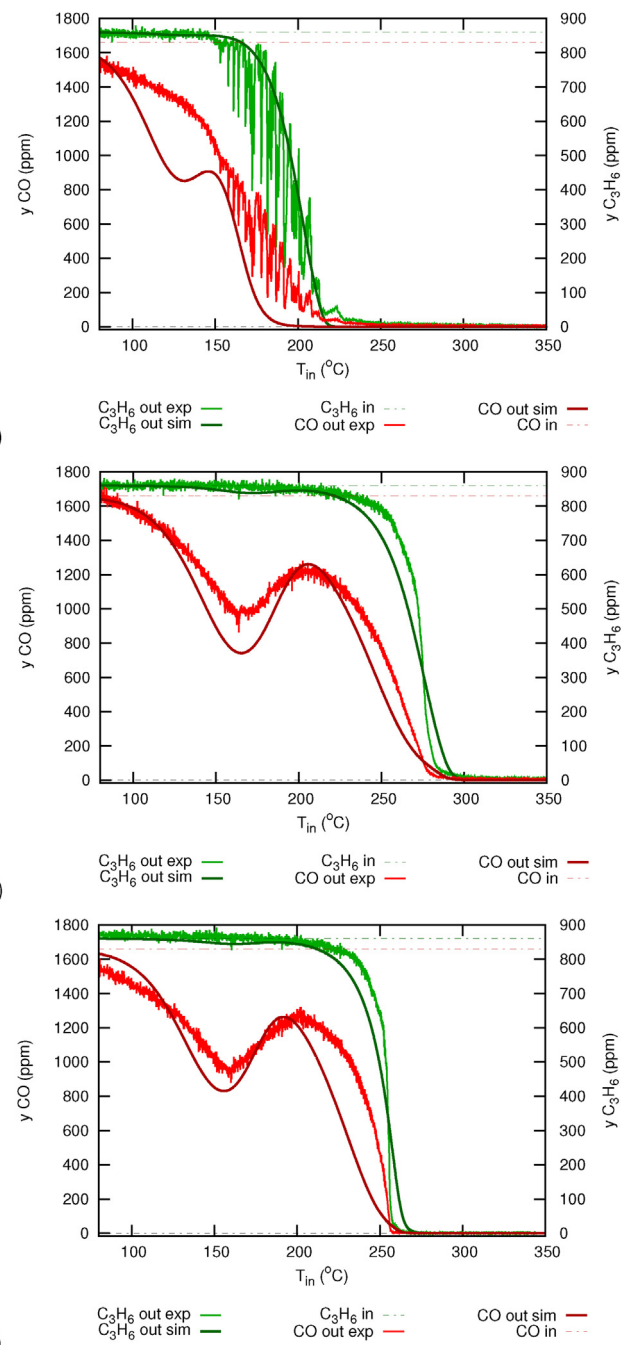


Fig. 5. Co-oxidation of propylene and CO with increased O₂ level representing slightly lean mixture (a) in the absence of NO, (b) in the presence of 600 ppm NO, (c) in the presence of 300 ppm NO. Feed gas composition: 1660 ppm CO, 860 ppm C₃H₆, 0.823 % O₂, 0/600/300 ppm NO, 7 % H₂O, 7 % CO₂, balance N₂.

models [22,23,27–29]. Such complex dynamic behavior is beyond the scope of this paper and capabilities of global kinetic models. The correctly predicted mean values of CO and C₃H₆ concentrations are thus considered as sufficient output of the global kinetic model.

Let us now discuss the mechanisms leading to such dependence on oxygen and NO. With the increasing O₂ concentration (Fig. 5), CO and C₃H₆ light-off occurs at lower temperatures than in the stoichiometric mixture (Fig. 4). The CO peak in the absence of NO (Fig. 5a) becomes quite small, however, Fig. 5b suggests again that NO strongly inhibits total C₃H₆ oxidation while the partial C₃H₆ oxidation to the surface intermediates is less affected. The higher coverage of surface

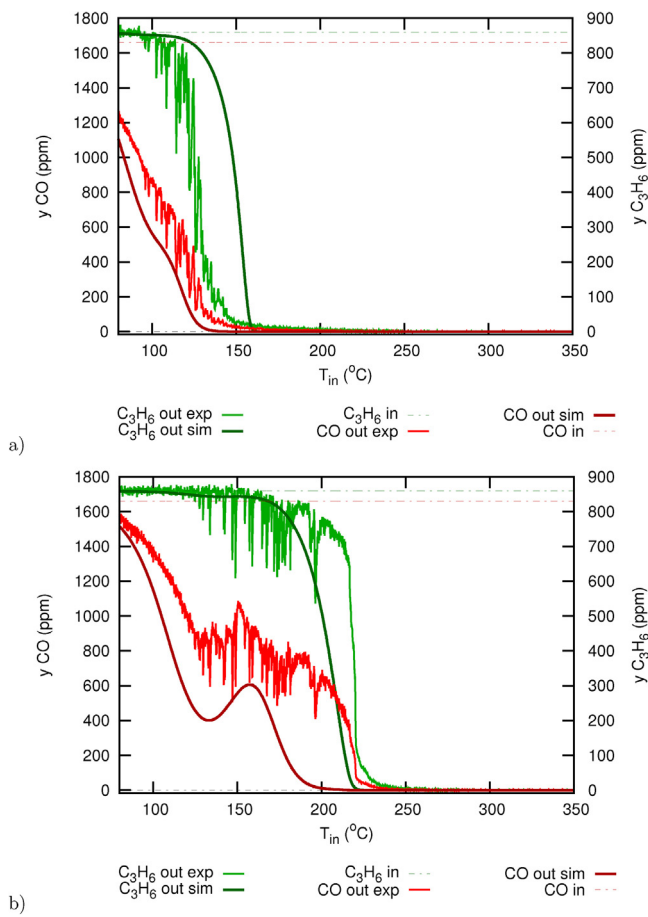


Fig. 6. Co-oxidation of propylene and CO in a fully lean mixture with large O₂ excess (a) in the absence of NO, (b) in the presence of NO. Feed gas composition: 1660 ppm CO, 860 ppm C₃H₆, 6.584 % O₂, 0/600 ppm NO, 7 % H₂O, 7 % CO₂, balance N₂.

intermediates then results in a stronger inhibiting effect on CO oxidation in the presence of NO. This is reflected in the difference between the inhibition coefficient $K_{inh,3}$ employed in the inhibition term G_1 and $K_{inh,16}$ employed in the inhibition term G_6 , see Table 5.

This effect of NO is confirmed also in the lean mixture with large O₂ excess (Fig. 6). The peak on CO light-off curve without NO almost diminishes and shrinks into a minor shoulder (Fig. 6a). However, the secondary CO peak is still clearly visible in the presence of NO (Fig. 6b).

The shrinking of the secondary CO peak with the increasing O₂ concentration observed in Figs. 4–6 suggests that formation of the C₃H₆ oxidation by-products (HCOO^{*} and CO) is less sensitive to O₂ concentration than the total C₃H₆ oxidation. This is reflected in the values of rate orders β_1 and β_2 with respect to oxygen, given in Table 5. The rate order β_2 smaller than one is used in the reaction rates R_6 and R_8 in Table 4. On the other hand, the experimental data suggest that the total oxidation of propylene, CO and surface intermediates to CO₂ product depends linearly on the oxygen concentration so that $\beta_1 = 1$, see the reaction rates R_1 , R_2 and R_7 in Table 4 and the value β_1 in Table 5. Such a combination of the rate orders leads to a considerable formation of by-products at low oxygen concentration, while total oxidation prevails at high oxygen concentration.

Fig. 8 shows the system behavior during subsequently repeated heating and cooling ramps. The complex shape of CO light-off curve is observed during the initial heat-up, however, the extinction curve as well as the second light-off curve are smooth. At the temperatures above ca. 230 °C, the CO conversion is almost identical on all three branches, except the small classic hysteresis loop between cooling and heating caused by a partial non-isothermality of the reactor [30]. At

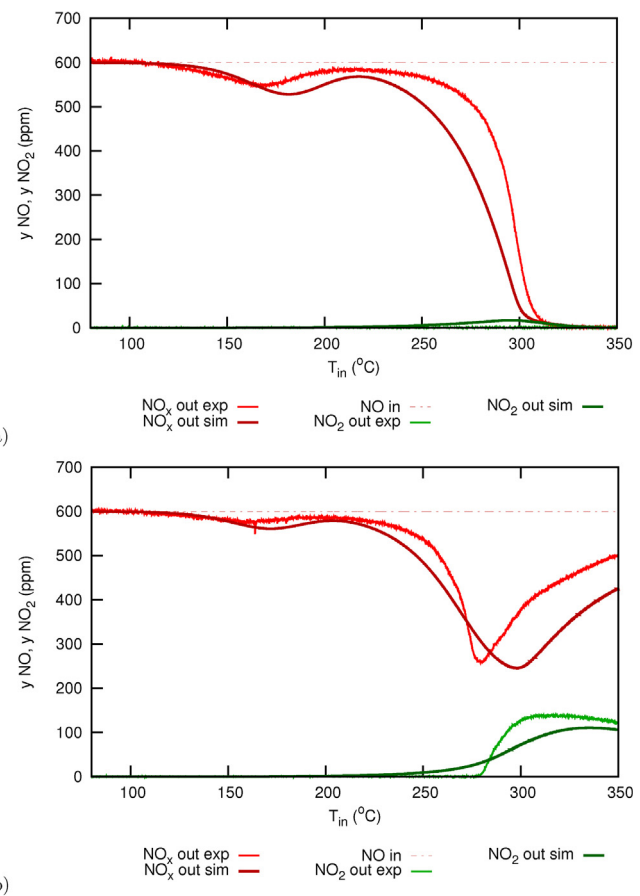


Fig. 7. Outlet NO_x concentrations during light-off experiments with (a) nearly stoichiometric mixture, (b) slightly lean mixture. Feed gas composition: 1660 ppm CO, 860 ppm C₃H₆, 0.440 % O₂ (a) / 0.8232 % O₂ (b), 600 ppm NO, 7 % H₂O, 7 % CO₂, balance N₂.

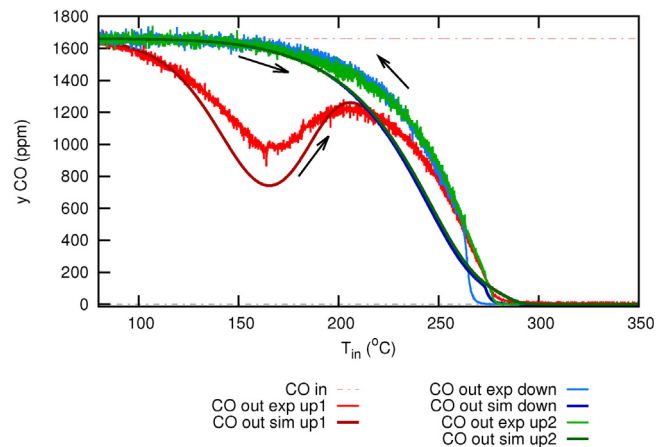


Fig. 8. Outlet CO concentration during subsequent heat-up and cool-down ramps. Feed gas composition: 1660 ppm CO, 860 ppm C₃H₆, 0.8232 % O₂, 600 ppm NO, 7 % H₂O, 7 % CO₂, balance N₂.

lower temperatures, however, an inverse hysteresis of CO conversion is observed due to transient nature of the hydrocarbon intermediates formation.

Let us remind that both formation and consumption reactions of the intermediates accelerate with temperature so that the steady-state coverage is reached much faster at higher temperatures. At low temperatures, the built-up of intermediates is quite slow, which results in a complex shape of the first CO light-off curve. However, the

intermediates are built readily on the extinction curve when cooling from higher temperatures, which results in an immediate inhibition of CO oxidation. When the temperature further decreases, the intermediates become stable and remain on the surface. The second heat-up curve then starts with a high coverage of intermediates, resulting in a strong inhibition of CO oxidation already from the beginning. CO conversion during the second light-off and extinction therefore coincide, except the small classical hysteresis window due to thermal effects mentioned earlier. It can be seen that the model consistently captures all the features in the system behavior (Fig. 8).

The intermediates build-up on the extinction curve is possible only in the presence of hydrocarbons. Therefore, if the oxidation experiment is terminated at high temperature and the catalyst is cooled down in air (which corresponds to the real situation after the car engine stops), the catalyst surface remains clean and the subsequent light-off exhibits again the complex behavior identical to the initial light-off curve.

With the developed mathematical model, actual surface coverage by the hydrocarbon oxidation intermediates during the experiment can be predicted. Fig. 9a shows the profiles of C_3H_6 oxidation intermediates represented by the coverage of model species $HCOO^*$ during the initial light-off in the absence of NO under excess of oxygen. At the beginning, the by-product is formed gradually and the surface coverage is uniform along the monolith in accordance with the uniform C_3H_6 concentration profile in gas phase (very small C_3H_6 conversion before its light-off). The maximum is achieved around 125 °C, when secondary CO peak occurs in the corresponding Fig. 6a. The oxidation of surface

intermediates accelerates significantly around 200 °C and leads to gradual clean-up of the surface. During this phase, the surface intermediates profile is uneven and the front section of the catalyst remains partly occupied up to relatively high temperature. The higher concentration of intermediates in the zone close to the inlet correlates with higher concentration of C_3H_6 in the gas phase. At higher temperatures, C_3H_6 is readily oxidized and its concentration quickly decreases along the monolith (z coordinate). The coverage profile in the presence of NO is depicted in Fig. 9b). In this case, the intermediates remain on the surface in a larger temperature window due to the more significant inhibition of total C_3H_6 oxidation. This is in line with the previously discussed effect of NO on the extent of the observed two-step CO light-off behavior (Fig. 5b).

5. Conclusions

The novel global kinetic model for CO and C_3H_6 oxidation developed and presented in this work is able to predict the extent of dual CO light-off effect on $Pt/\gamma-Al_2O_3$ catalyst depending on CO, C_3H_6 , O₂ and NO concentrations. Two reaction pathways contributing to an increase of CO concentration are included: (i) accumulation of C_3H_6 oxidation intermediates on the catalyst surface, leading to progressively increasing inhibition of CO oxidation, and (ii) CO formation as a by-product of partial propylene oxidation. The latter pathway was found to play only minor role.

The developed model represents a useful software tool enabling more precise prediction of pollutant conversion after cold start and it can assist in finding proper control strategies for minimization of the light-off delays in oxidation and three-way catalysts for the automotive exhaust gas aftertreatment.

Acknowledgements

The work was financially supported by the Czech Science Foundation (project GA 17-26018S) and specific university research (MSMT No 20-SVV/2017). The authors thank to Volker Schmeißer, Michel Weibel and Simone Dieterich at Daimler AG for fruitful discussion and feedback from practical application in the automotive exhaust gas aftertreatment.

References

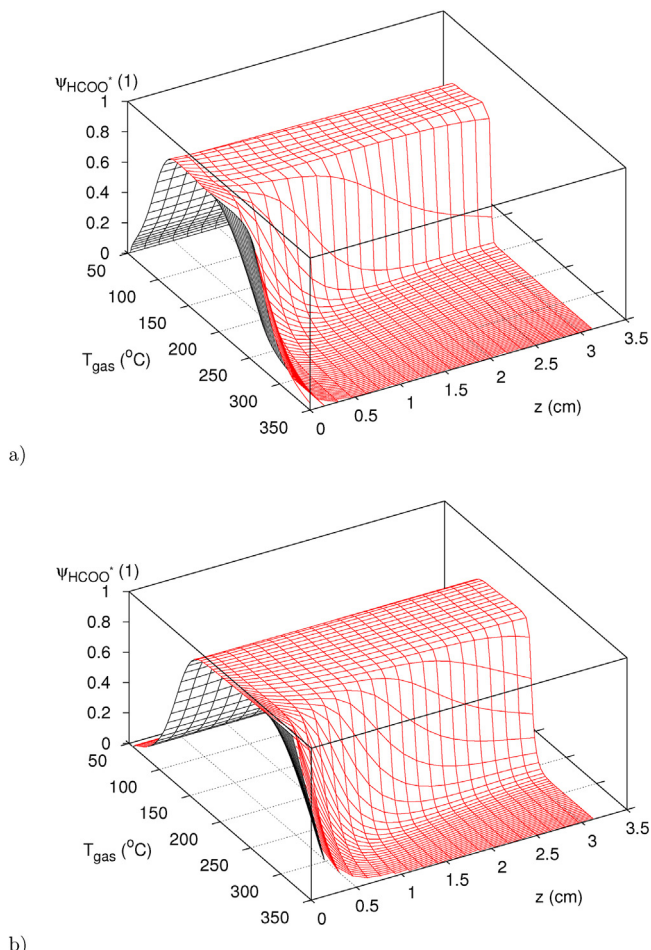


Fig. 9. Predicted surface coverage by $HCOO^*$ species during initial light-off of propylene and CO in a lean mixture (a) in the absence of NO, (b) in the presence of NO. Feed gas composition: 1660 ppm CO, 860 ppm C_3H_6 , 6.584 % O₂, 0/600 ppm NO, 7 % H₂O, 7 % CO₂, balance N₂.

- [1] S.E. Voltz, C.R. Morgan, D. Liederman, S.M. Jacob, Kinetic study of carbon monoxide and propylene oxidation on platinum catalysts, *Ind. Eng. Chem. Prod. Res. Dev.* 12 (1973) 294–301.
- [2] S.H. Oh, J.C. Cavendish, Transients of monolithic catalytic converters: response to step changes in feedstream temperature as related to controlling automobile emissions, *Ind. Eng. Chem. Prod. Res. Dev.* 21 (1982) 29–37.
- [3] A. Güttenke, D. Chatterjee, M. Weibel, B. Krutzsch, P. Kočí, M. Marek, I. Nova, E. Tronconi, Current status of modeling lean exhaust gas aftertreatment catalysts, *Adv. Chem. Eng.* 33 (2007) 103–211.
- [4] M.J. Patterson, D.E. Angove, N.W. Cant, The effect of carbon monoxide on the oxidation of four C₆ to C₈ hydrocarbons over platinum, palladium and rhodium, *Appl. Catal. B* 26 (2000) 47–57.
- [5] M. Khosravi, A. Abedi, R.E. Hayes, W.S. Epling, M. Votsmeier, Kinetic modelling of Pt and Pt:Pd diesel oxidation catalysts, *Appl. Catal. B* 154–155 (2014) 16–26.
- [6] M.J. Hazlett, W.S. Epling, Spatially resolving CO and C_3H_6 oxidation reactions in a $Pt/\gamma-Al_2O_3$ model oxidation catalyst, *Catal. Today* 267 (2016) 157–166.
- [7] M.J. Hazlett, M. Moses-Debusk, J.E. Parks, L.W. Allard, W.S. Epling, Kinetic and mechanistic study of bimetallic Pt-Pd/ $\gamma-Al_2O_3$ catalysts for CO and C_3H_6 oxidation, *Appl. Catal. B* 202 (2017) 404–417.
- [8] W. Lang, P. Laing, Y. Cheng, C. Hubbard, M.P. Harold, Co-oxidation of CO and propylene on Pd/CeO₂-ZrO₂ and Pd/ $\gamma-Al_2O_3$ monolith catalysts: a light-off, kinetics, and mechanistic study, *Appl. Catal. B* 218 (2017) 430–442.
- [9] K. Daneshvar, R.K. Dadi, D. Luss, V. Balakotaiah, S.B. Kang, C.M. Kalamaras, W.S. Epling, Experimental and modeling study of CO and hydrocarbons light-off on various Pt-Pd/ $\gamma-Al_2O_3$ diesel oxidation catalysts, *Chem. Eng. J.* 323 (2017) 347–360.
- [10] M. Herrmann, R.E. Hayes, M. Votsmeier, Propene induced reversible deactivation effects in diesel oxidation catalysts, *Appl. Catal. B* 220 (2018) 446–461.
- [11] A.K. Agarwal, A.P. Singh, R.K. Maurya, Evolution, challenges and path forward for low temperature combustion engines, *Prog. Energy Combust. Sci.* 61 (2017) 1–56.
- [12] A.J. Torregrosa, A. Broatch, A. García, L.F. Mónico, Sensitivity of combustion noise

and NO_x and soot emissions to pilot injection in PCCI Diesel engines, *Appl. Energy* 104 (2013) 149–157.

[13] X. Lu, D. Han, Z. Huang, Fuel design and management for the control of advanced compression-ignition combustion modes, *Prog. Energy Combust. Sci.* 37 (2011) 741–783.

[14] G.C. Koltsakis, P.A. Konstantinidis, A.M. Stamatelos, Development and application range of mathematical models for 3-way catalytic converters, *Appl. Catal. B* 12 (1997) 161–191.

[15] S. Salomons, R.E. Hayes, M. Votsmeier, A. Drochner, H. Vogel, S. Malmberg, J. Gieshoff, On the use of mechanistic CO oxidation models with a platinum monolith catalyst, *Appl. Catal. B* 70 (2007) 305–313.

[16] J. Chen, H. Yang, N. Wang, Z. Ring, T. Dabros, Mathematical modeling of monolith catalysts and reactors for gas phase reactions, *Appl. Catal. A* 345 (2008) 1–11.

[17] J. Koop, O. Deutschmann, Detailed surface reaction mechanism for Pt-catalyzed abatement of automotive exhaust gases, *Appl. Catal. B* 91 (2009) 47–58.

[18] K. Hauff, U. Tuttles, G. Eigenberger, U. Nieken, A global description of DOC kinetics for catalysts with different platinum loadings and aging status, *Appl. Catal. B* 100 (2010) 10–18.

[19] R. Raj, M.P. Harold, V. Balakotaiah, Steady-state and dynamic hysteresis effects during lean co-oxidation of CO and C₃H₆ over Pt/Al₂O₃ monolithic catalyst, *Chem. Eng. J.* 281 (2015) 322–333.

[20] J.M. Harmsen, J.H. Hoebink, J.C. Schouten, Transient kinetic modeling of the ethylene and carbon monoxide oxidation over a commercial automotive exhaust gas catalyst, *Ind. Eng. Chem. Res.* 39 (2000) 599–609.

[21] J.M. Harmsen, J.H. Hoebink, J.C. Schouten, Acetylene and carbon monoxide oxidation over a Pt/Rh/CeO₂/Al₂O₃ automotive exhaust gas catalyst: kinetic modeling of transient experiments, *Chem. Eng. Sci.* 56 (2001) 2019–2035.

[22] P. Kočí, M. Kubíček, M. Marek, Modelling of TWC monolith converters with microkinetics and diffusion in the washcoat, *Ind. Eng. Chem. Res.* 43 (2004) 4503–4510.

[23] P. Kočí, V. Nevoral, M. Záhrubský, M. Kubíček, M. Marek, Nonlinear dynamics of automobile exhaust gas converters: the role of nonstationary kinetics, *Chem. Eng. Sci.* 59 (22–23) (2004) 5597–5605.

[24] A.S. Kota, R.K. Dadi, D. Luss, V. Balakotaiah, Analysis of light-off during oxidation of reactant mixtures on Pt/Al₂O₃ using micro-kinetic models, *Chem. Eng. Sci.* 166 (2017) 320–333.

[25] A. Arvajová, P. Kočí, V. Schmeißer, M. Weibel, The impact of CO and C₃H₆ pulses on PtO_x reduction and NO oxidation in a diesel oxidation catalyst, *Appl. Catal. B* 181 (2016) 644–650.

[26] M. Dudák, V. Novák, P. Kočí, M. Marek, P. Blanco-García, G. Jones, Prediction of diffusivity and conversion of n-decane and CO in coated Pt/γ-Al₂O₃ catalyst depending on porous layer morphology, *Appl. Catal. B* 150–151 (2014) 446–458.

[27] J. Kapička, M. Marek, Oscillations on individual catalytic pellets in a packed bed: CO oxidation on Pt/Al₂O₃, *J. Catal.* 119 (1989) 508–511.

[28] C.D. Lund, C.M. Surko, M.B. Maple, S.Y. Yamamoto, Model discrimination in oscillatory CO oxidation on platinum catalysts at atmospheric pressure, *Surf. Sci.* 459 (3) (2000) 413–425.

[29] J. Sá, D.L. Abreu Fernandes, F. Aiouache, A. Goguet, C. Hardacre, D. Lundie, W. Naeem, W.P. Partridge, C. Stere, SpaciMS: spatial and temporal operando resolution of reactions within catalytic monoliths, *Analyst* 135 (2010) 2260–2272.

[30] L.L. Hegedus, S.H. Oh, K. Baron, Multiple steady states in an isothermal, integral reactor: the catalytic oxidation of carbon monoxide over platinum-alumina, *AIChE J.* 23 (5) (1977) 632–642.